THE JOURNAL OF PHYSICAL CHEMISTRY C

Article

Cite This: J. Phys. Chem. C 2019, 123, 7475−7485

pubs.acs.org/JPCC

Isotope Effects Reveal the Template Influence on the Crystal Growth of a Metal−Halide Network

Feier Hou and James D. Martin*

Department of Chemistry, North Carolina State University, Raleigh, North Carolina 27695-8204, United States

Supporting Information

ABSTRACT: Crystallization requires the organization of matter into structures with long-range translational order. However, because crystal growth exhibits non-Arrhenius kinetics, it is not possible to apply classical transition state theory to decipher mechanistic details of the crystallization process. With our recently discovered transition zone theory of crystallization, for the first time, it is possible to extract enthalpic and entropic activation parameters for crystal growth from which chemically/physically meaningful mechanistic information is obtained. Here, we measured the respective temperature-dependent crystal growth rates for d_0, d_1, d_9, and d_{10} isotopomers of the halozeotype CZX-1 to explore how the templating cation impacts the rate of crystal growth. The isotopic dependence of the Kauzmann temperature, T_K, and the enthalpic and entropic activation parameters reveal that the mechanism of crystal growth is controlled by both inertial (mass) effects of the template and hydrogen bonding between the template and the metal−halide network. In addition to revealing the role of template−framework interactions for crystal growth of the specific CZX-1 material, this detailed isotope effect study provides an experimental and theoretical framework with which to evaluate details of other condensed-matter reactions.

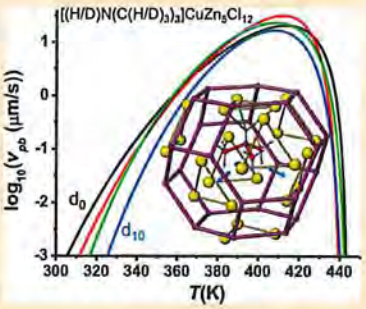

INTRODUCTION

Whether for purposes of aesthetics or diverse applications from pharmaceuticals to advanced electronic materials, the mechanistic processes involved in crystal growth have been of major interest to scientists and engineers for centuries.[1−6] However, deciphering the physical/chemical processes that determine crystal growth is complex, being the result of cooperative, as opposed to individual, particle interactions, as well as both intrinsic and extrinsic factors.

To understand crystallization, it is important to deconvolute intrinsic and extrinsic effects. Extrinsic control of crystallization has been achieved by functional group modification of nucleation templates or growth modifiers,[7,8] solvent effects,[9−11] or with the use of physical masks, confined environments, or deposition of layered superstructures.[12,13] Intrinsic effects, including the size and shape of the species crystallizing and the corresponding intermolecular interactions, primarily control the crystal structure itself; e.g., ionic radius ratios determine NaCl versus CsCl structure types, secondary building units direct metal−organic framework structures,[14] and templates determine diverse zeolite structures.[15]

While it is generally accepted that intrinsic bonding/packing factors should impact the rate and thus mechanism of crystallization, they are frequently masked by extrinsic effects (e.g., rate-limiting solvent−solute interactions[16−19]). To eliminate as many extrinsic influences as possible, so as to decipher intrinsic atomic and molecular control of crystallization, we have focused on crystallization of congruent melts.[20,21] However, only using congruently melting systems imposes strict limits with respect to possible modifications to test hypotheses regarding the influence of specific structures and bonding features on the mechanism of crystal growth.

Herein, we suggest that kinetic isotope effect (KIE) investigations can provide a unique window into intrinsic control of crystal growth. Isotopic changes to components of a system that are directly involved in its transition configurations significantly change the rate of the reaction[22] although comparatively few studies of isotope effects are reported for crystallization.[16,23−25]

KIEs traditionally are determined by the ratio of rate constants when atoms in the reactant are substituted with their isotopes, e.g., k_H/k_D, which is valid when considering reactions that follow Arrhenius or Eyring-type kinetics[26] for which reaction rates monotonically increase with increasing temperature. This tends to be the case for reactions in dilute media, i.e., gas phase or dilute solution. However, crystal growth from the melt, a condensed-matter reaction, exhibits notably non-Arrhenius behavior, with a maximum in the rate observed at T_{max}, between the glass-transition temperature, T_g, and the melting temperature, T_m.[27,28] As such, the ratio of relative rates of isotopically substituted materials depends significantly on the temperature range over which the rates are measured. Thus, to understand the chemical/physical significance of any isotope effects on crystal growth rates, it is necessary to evaluate relative activation parameters rather than relative rate constants. Furthermore, to extract meaningful isotope effects from reaction rate measurements, it is critical to independently

Received: February 10, 2019
Published: February 26, 2019

DOI: 10.1021/acs.jpcc.9b01334
J. Phys. Chem. C 2019, 123, 7475−7485

evaluate singular processes, i.e., crystal growth or nucleation. Different extents of nucleation for otherwise equivalent reaction conditions dramatically change apparent crystallization rates. Herein, we exploit temperature-/time-resolved synchrotron X-ray diffraction (TtXRD) methods, along with differential scanning calorimetry (DSC) methods, to measure the isotope effect on the rate of crystal growth, independent of the rate of nucleation.

The halozeotype CZX-1, $[HNMe_3][CuZn_5Cl_{12}]$,[29] provides an excellent system with which to use isotope effects to decipher the intrinsic role of a templating cation on the mechanism of crystallization. CZX-1 exhibits a sodalite-type structure, with the $[HNMe_3]^+$ cation disordered about four tetrahedrally distributed orientations, hydrogen-bonded to sets of three chlorides in the interior of the cages; Figure 1. By

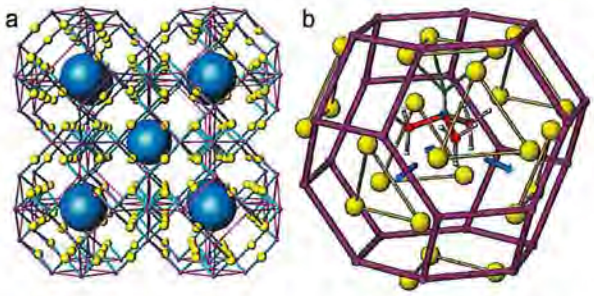

Figure 1. Structure of CZX-1 ($[HNMe_3][CuZn_5Cl_{12}]$) showing (a) the metal–halide network structure with the methylammonium templates represented as large blue spheres and (b) a single β-cage with one orientation of the template shown for which hydrogen bonding is indicated by green lines and the three other possible template orientations represented by blue arrows. (Cu/Zn atoms and framework, magenta; M–Cl bonds, turquoise; chloride, yellow; carbon, red; nitrogen, blue; hydrogen, white.)

systematic H/D isotopic substitution, the d_0-$[HN(CH_3)_3]^+$, d_1-$[DN(CH_3)_3]^+$, d_9-$[HN(CD_3)_3]^+$, and d_{10}-$[DN(CD_3)_3]^+$ templates make it possible to probe the influence of the moment of inertia for template reorientation on the rate of crystallization by comparing the d_0 versus d_9 and d_1 versus d_{10} isotopomers and probe the influence of template–framework hydrogen bonding on crystallization by comparing the d_0 versus d_1 and d_9 versus d_{10} isotopomers.

Synchrotron X-ray and neutron scattering studies of CZX-1 reveal that even in the amorphous state, >5 nm structural signatures of the sodalite-type network remain.[30,31] In this system, as also observed for numerous MX_2 network phases,[32] there is no significant difference in the observed average short-range contacts of crystalline and liquid phases (D–Cl = 2.6 Å, M–Cl = 2.3 Å, or Cl–Cl = 3.8 Å). The near equivalence of short-range order between the crystal and melt phase is predictable given the less than 10% decrease in density between crystals at room temperature and a melt. Note that a 10% reduction in density corresponds to a maximum increase in average short-range contacts of 3.2%, which is an order of magnitude less than 36% increase required to break Zn–Cl bonds (the Zn–Cl distance in CZX-1 is 2.3 Å and the sum of the Zn and Cl van der Waals radii (1.39 Å + 1.75 Å) is 3.14 Å). As such, molten CZX-1, like other MX_2-type network materials, exhibits what has been described as a chemically and topologically ordered network.[32]

A critical consequence of the high structural similarity between the liquid and crystalline structures of CZX-1 is that no clearly defined interface between the melt and crystal can exist, i.e., the difference between a melt and a crystal is defined relative to the long-range order since the short- and intermediate-range orders of the melt and crystal are essentially equivalent. Recognition that there is no clearly defined interface between the melt and crystal phases requires a re-examination of classical models of crystal growth, which presume crystallization to be controlled by the attachment/detachment of matter across a liquid/crystal interface. Upon melting, the density reduction is simply not sufficient to break the Zn–Cl network bonding, a requirement for "detachment." Therefore, unlike crystallization from dilute media, for melt crystallization there is nothing to attach to or detach from. Instead, crystallization must be controlled by the reorganization of the intermediate-range-ordered molten network into a long-range-ordered crystalline network.

We suggest that the process of developing long-range order from the intermediate-range order must be governed by the entropy of activation. An understanding of the entropic control of crystal growth led to our recent development of the transition zone theory of crystallization, TZT_c,[20] a condensed-matter analog to Eyring's transition state theory.[26] This theory originates from an incorporation of Kauzmann's description of the temperature dependence of configurational entropy[33] and Adam and Gibbs' description of the temperature dependence of cooperativity[34] into classical conceptions of activated processes. Importantly, TZT_c yields both enthalpic and entropic activation parameters for crystal growth, which, for the first time, allows a detailed analysis of the isotope effects of the rate of crystal growth from a melt.

Before applying TZT_c to the evaluation of the isotope effects of the crystal growth rate of CZX-1, it may be useful to briefly review the classical interface controlled growth (ICG) model and contrast it with TZT_c, which we suggest addresses numerous drawbacks of the classical model.

BACKGROUND THEORY

Interface Controlled Growth (ICG) Model. In the classic review of the theory describing "crystal growth from a melt",[28] the rate of crystal growth is described based on a presumption of the competition between the rate of attachment ($r_a = \nu \exp(-\Delta G_a^{\ddagger}/RT)$) and the rate of detachment ($r_d = \nu \exp(-(\Delta G_c + \Delta G_a^{\ddagger})/RT)$), where ν is an attempt frequency, R is the gas constant, T is temperature in Kelvin, $\Delta G_a^{\ddagger}$ and ΔG_c are the free energy differences between the liquid and activated state, and the crystal, respectively. The growth rate, Y, then is said to be the product of these, multiplied by the thickness per molecular layer, a_0, and by the fraction of the sites on the crystal surface available for attachment, f, yielding the general rate (eq 1)

$$Y = fa_0\nu \exp(-\Delta G_a^{\ddagger}/RT)[1 - \exp(-\Delta G_c/RT)] \quad (1)$$

Notably describing the rate of crystal growth to be the product of attachment and detachment presumes crystallization to be a thermodynamically reversible process. However, that assumption is only correct at the liquidus temperature. At any lower temperatures, crystallization is an irreversible first-order process. The microscopic reversibility assumption of an attachment/detachment model is based on an individual particle-based perspective and does not take the collective

DOI: 10.1021/acs.jpcc.9b01334
J. Phys. Chem. C 2019, 123, 7475–7485

effect of the lattice into account. Furthermore, even in molecular systems, the relationship of the forward and reverse rate constants (equivalent to the said attachment/detachment of crystal growth) determines the equilibrium constant, but it does not change the rate of the reaction. In addition, f and a_0 are not measurable parameters with respect to crystal growth from a melt since, as noted above, neither a "molecular layer" nor "sites for attachment" can be defined when the melt is already a chemically and topologically ordered network.

A version of the ICG model suggests that at large undercooling, ΔG_c can be presumed to be large with respect to RT, simplifying eq 1 to eq 2, for which a plot of $\ln(Y)$ versus $1/T$ is suggested to afford the enthalpy of activation, $\Delta H_a^{\ddagger}$, and if f, a_0, and ν are known, the entropy of activation, $\Delta S_a^{\ddagger}$, analogous to the Eyring analysis of transition state theory.[35]

$$Y = f a_0 \nu \exp(-\Delta H_a^{\ddagger}/RT) \exp(\Delta S_a^{\ddagger}/R) \quad (2)$$

The simplifying assumption of ΔG_c being large with respect to RT becomes less valid for systems with small, ΔG_c, i.e., those whose liquid and crystalline structures are most similar. Furthermore, the temperature-independent enthalpic and entropic parameters of eq 2 are inconsistent with Kauzmann's description of configurational entropy[33] and Adam and Gibbs' description of cooperativity.[34]

A modification to eq 1 was introduced by Turnbull and Cohen,[36] suggesting that the activated term can be related to the diffusion coefficient for transport across a melt−crystal interface. Using the Stokes−Einstein relationship to define the diffusion, the growth rate is alternatively described by eq 3.

$$Y = \frac{f k_B T}{3\pi a_0^{\,2} \eta}\left[1 - \exp\left(\frac{-\Delta G_c}{RT}\right)\right] \quad (3)$$

where k_B is Boltzmann's constant and η is the viscosity. Based on suggested different interfacial characteristics, several versions of eq 3 are described as the "normal model", the "screw dislocation model," and the "two-dimensional (2-D) surface nucleation growth model."[37,38] As noted above, the essentially equivalent short- and intermediate-range order of a liquid's chemically and topologically ordered network and a crystal's long-range-ordered crystalline network both raise questions as to the definition of an interface between a crystal and its congruent melt and the need for any substantive mass transport, i.e., diffusion. In addition, above the glass transition, it is experimentally recognized that viscous relaxation is a faster process than the rate of growth,[39,40] which, from a mechanistic perspective, means viscous relaxation cannot be rate determining to the slow step of crystal growth.

Each of the above modifications of the ICG model can be used to fit crystal growth data to varying degrees of success and generally over limited temperature regimes. To account for fits to only limited temperature ranges, conventional wisdom suggests that deviations, such as the non-Arrhenius region, are the result of the existence of "multi-step processes" with "cross-over temperatures" between them. However, the addition of a subsequent slow step to transform the same melt to the same crystal cannot kinetically compete with a primary fast process and thus will not slow the rate at high temperature. Conceivably, under certain reaction conditions, formation of an intermediate could be competitive with direct growth. But then some "non-Arrhenius" process would need to convert that intermediate to the crystalline product at a slower rate than the direct liquid to crystal transformation to account for the slowed rate of growth as T_m is approached. Specifically in the CZX-1 system, experimental measurements, even in the slow-growth temperature range, demonstrate an isosbestic transition from liquid to crystal, their abundance crossing at 50% transformation, indicative of the absence of any intermediates in the crystal growth process.[41]

Thus, there is a need for a substantially different model to describe the rate of melt-crystal growth that: (a) is consistent with a first-order irreversible process; (b) recognizes that crystallization from a melt involves the transformation of intermediate-range order into long-range order rather than requiring diffusion of matter by attachment to/detachment from an interface; and (c) recognizes for condensed matter that the configurational entropy and cooperativity of the system are significantly temperature dependent.

Transition Zone Theory of Crystallization (TZT$_c$). Because the entropy of activation to transform intermediate-range order into long-range order for melt crystallization should always be negative, and thus $T\Delta S_c^{\ddagger}$ should become increasingly unfavorable at higher temperatures, we submit that the entropy of activation is likely to be the primary factor controlling the diminished melt → crystal growth rate as $T > T_{max}$. To address this, in our recent development of transition zone theory (TZT),[20] we integrated Kauzmann's description of the temperature dependence of configurational entropy[33] and Adam and Gibbs' concepts of temperature-dependent cooperativity[34] into Eyring's transition state theory (TST)[26] so as to be able to describe the activation barrier in condensed phase processes.

TST describes the rate constant of a reaction to be the product of a molecular collision attempt frequency, $\frac{k_B T}{h}\nu$, and the probability a reactant is activated to the transition state, $\exp\left(\frac{-\Delta G^{\ddagger}}{RT}\right)$. Adam and Gibbs previously noted that the model of single particles traversing the activation barrier is inadequate to describe condensed phase reactions. Instead, cooperative rearrangements of groups of particles are required[34] and thus a transition zone, TZ, instead of a transition state. Correspondingly, instead of a Boltzmann distribution of atomic or molecular collisions, condensed phase reactions can be described as a Boltzmann-type distribution of interacting phonons.[42,43] Thus, for TZT$_c$, we submit that the prefactor is the product of the number of phonons leading to the transition zone, $\frac{k_B T}{h\nu}$, and the velocity of the transition zone, $\lambda\nu$, for which λ is equal to twice the average lattice constant (i.e., approximately the first Brillion zone of the allowed lattice vibrations). Like for TST, in TZT$_c$, the probability that the reactant (the relaxed melt) is activated to the transition zone is governed by the free energy of activation, $\Delta G_c^{\ddagger}$. However, unlike TST, in the condensed phase, both the enthalpy $\Delta H_c^{\ddagger}$ and entropy $\Delta S_c^{\ddagger}$ of activation are significantly temperature dependent.

Described as the Kauzmann paradox,[33] the temperature dependence of a liquid's configurational entropy, S_{liq}, is greater than that of its crystalline phase, S_{xtl}. As a result, there is a temperature, T_K, at which the configurational entropy of the liquid and crystal become equivalent, i.e., $\Delta S_c = 0$. Boltzmann's definition of entropy states $S = R\ln(W)$, where W is the number of configurations of a system. At T_K, if the reactant liquid and product crystal exhibit an equivalent and small number of configurations, it is reasonable to assume that a

DOI: 10.1021/acs.jpcc.9b01334
J. Phys. Chem. C 2019, 123, 7475−7485

similar small number of configurations describe the TZ. Since $\Delta S^{\ddagger}$ is governed by the ratio of the number of configurations of the TZ, $W^{\ddagger}$, to the number of reactant configurations (melt), W_{rct}, as $T \to T_K$, $\frac{W^{\ddagger}}{W_{\mathrm{rct}}} \to 1$ and thus $\Delta S_c^{\ddagger} \to 0$. By contrast, at T_m, there remains a small number of crystalline configurations and thus we assume a small number of TZ configurations. But the higher-temperature liquid exhibits a comparatively large number of configurations. Thus, as $T \to T_m$, $\frac{W^{\ddagger}}{W_{\mathrm{rct}}} = \frac{\mathrm{few}}{\mathrm{many}} \to 0$ and thus $\Delta S^{\ddagger} \to -\infty$. In TZT$_c$, we model this temperature dependence of the entropy of activation as $\Delta S_c^{\ddagger} = \Delta S_c^{*}\left(\frac{T - T_K}{T_m - T}\right)^{z_c}$, where ΔS_c^{*} is an intrinsic term, which indicates the extent of structural organization necessary for crystallization, and z_c is a semiempirical factor that scales the temperature dependence of the system. Ongoing evaluation of more than 30 diverse systems ranging from the fragile OTP to strong SiO_2 finds z_c apparently to be correlated with the S_c^{*} parameter, $z_c \approx -R/\Delta S_c^{*}$. Based on the Boltzmann entropy relationship, this suggests that z_c is reflective of a change in the ratio of configurations between the relaxed liquid and crystallization TZ.

The Kauzmann condition also impacts the enthalpy of activation, $\Delta H_c^{\ddagger}$. The $\Delta H_c^{\ddagger}$ is dominated by the energy required for making, breaking, or rearranging bonding interactions in a given transformation. As a reaction system approaches T_K, the loss of configurational microstates requires an increased size of the cooperative region for each activation event. Thus, consistent with the model proposed by Adam and Gibbs,[34] $\Delta H^{\ddagger}$ should be proportional to the size of the cooperative regions. If a liquid could be supercooled to T_K, the entire sample would need to transform as a single cooperative region, essentially an impossible condition, i.e., as $T \to T_K$, $\Delta H_c^{\ddagger} \to \infty$. With increasing temperature, the size of the transforming cooperative regions decreases, with a corresponding decrease in $\Delta H_c^{\ddagger}$. In TZT$_c$, we use a classic Adam–Gibbs cooperativity expression to describe the enthalpic temperature dependence, $\Delta H_c^{\ddagger} = \Delta H_c^{*}\left(\frac{T}{T - T_K}\right)$, where ΔH^{*} is a material-specific parameter that correlates with the strength of the bonding (intermolecular interactions) in the material.

Together, these yield the TZT$_c$ expression given in eq 4, where v_{pb} is the velocity of the crystallization phase boundary.

$$v_{pb} = \lambda \frac{k_B T}{h} \exp\left(\frac{-\Delta H_c^{*}}{R(T - T_K)}\right) \exp\left(\frac{\Delta S_c^{*}}{R}\left(\frac{T - T_K}{T_m - T}\right)^{z_c}\right) \quad (4)$$

As described in a prior work, TZT$_c$ accurately describes the non-Arrhenius temperature dependence of crystal growth rates for a diverse set of materials.[20] Notably, the single TZT$_c$ expression provides more accurate fits to the crystallization data of a series of oxides[44] than could be achieved when trying to distinguish between various ICG models.[45] Having established an expression that describes the rate of crystal growth based on the physical/measurable parameters (λ, T_K, T_m), an enthalpic and entropic activation parameter (ΔH_c^{*}, ΔS_c^{*}), and with only one somewhat empirical parameter, z_c, in this work we investigate whether the TZT$_c$ expression can decipher subtle changes in the mechanistic parameters resulting from isotopic substitution of components in the reaction system.

METHODS

Material Preparation and Characterization. All manipulations were performed under an inert N_2 atmosphere in a glovebox or using vacuum lines. d_0-$HN(CH_3)_3Cl$ (Aldrich) and d_{10}-$DN(CD_3)_3Cl$ (Cambridge Isotope Laboratories) were purified via double sublimation at 403 K prior to use. d_1-$DN(CH_3)_3Cl$ and d_9-$HN(CD_3)_3Cl$ were prepared by bubbling $N(CH_3)_3$ (Matheson) or $N(CD_3)_3$ (Cambridge Isotope Laboratories) gas into 35 wt % DCl/D_2O (Aldrich) or 37.1 wt % HCl/H_2O (Fisher Scientific) solutions, respectively, followed by evaporation of the solvents at 373 K and sublimation at 403 K. The identity of the sublimed (H/D)$N(C(H/D)_3)_3Cl$ was confirmed by powder X-ray diffraction (PXRD, INEL CPS-120). $ZnCl_2$ (Aldrich) was purified by triple sublimation at 623 K prior to use. The $ZnCl_2$ was confirmed to be the anhydrous δ-phase by PXRD and by differential scanning calorimetry (DSC, TA Instruments Q2000) for which a congruent melt at 590 K is observed. CuCl was prepared and purified according to previously reported procedures.[46] The isotopically substituted variants of CZX-1 were prepared by melting the respective d_0-, d_1-, d_9-, or d_{10}-substituted trimethylamonium chloride salt with stoichiometric proportions of CuCl and $ZnCl_2$ with a molar ratio of 1:1:5.[29] The purity of the synthesized CZX-1 samples was confirmed by DSC, ensuring a narrow melting range consistent with a congruent melt, for which the T_m values of the new d_1, d_9, and d_{10} species were determined. The lattice constants of d_0-CZX-1 were previously reported based on single-crystal X-ray diffraction[29] and those of the d_1 to d_{10} isotopomers were measured by PXRD.

Measurement of the Kauzmann Temperature. The Kauzmann temperature, T_K, of each d_0-, d_1-, d_9-, and d_{10}-CZX-1 isotopomer was measured by temperature-modulated DSC (TA Instruments Q2000) (TMDSC). A 10–20 mg sample, sealed in a 1 mm I.D. fused silica capillary (Charles Supper Co., Natrick, MA), was melted at 523 K and quenched in liquid N_2 to form a glass ($T_g \sim 303$ K). The heat capacity, C_p, of the sample was measured as it was heated and cooled at a rate of 5° min^{-1} with a modulation of ±0.5° min^{-1} through the temperature range 253 K → 523 K → dwell 5 min → 298 K → 523 K. The temperature dependence of C_p of both liquid and crystalline phases was fit to a reciprocal function of temperature, and the temperature dependence of $\Delta C_p = C_{p,\mathrm{liq}} - C_{p,\mathrm{xtl}}$ is calculated from the fitted lines.[47] The entropy difference between the liquid and the solid at temperature T can be expressed by eq 5[48]

$$\Delta S = \frac{\Delta H_m}{T_m} - \int_T^{T_m} \frac{\Delta C_p}{T}\, dT \quad (5)$$

where ΔH_m is the enthalpy of melting, measured by integration of the melting peak from the standard DSC. T_K is solved for as the temperature at which $\Delta S = 0$. The reported T_K is the result of the average of five to ten TMDSC measurements for each sample.

Isothermal Crystallization (DSC). Analogous to DSC isothermal crystallization methods previously reported to obtain kinetic data for the crystallization of d_0-CZX-1,[41] approximately 15–35 mg samples of CZX-1 were sealed into high-pressure stainless steel DSC pans with gold foil seals (PerkinElmer product No. B0182901). The samples were melt-crystal cycled five times between 313 and 503 K at a constant rate of 5° min^{-1} before isothermal crystallization

DOI: 10.1021/acs.jpcc.9b01334
J. Phys. Chem. C 2019, 123, 7475–7485

experiments were performed to remove heterogeneous nucleation sites and ensure uniform thermal contact between the pan and sample. For isothermal hot crystallization, the samples were again heated to 503 K, held at the melt isotherm for 5 min, and then quenched to a crystallization isotherm (T_{iso}) of between 408 and 435 K at a maximum instrumental cooling rate of ~40° min^{-1}. For isothermal cold crystallization, the sample was heated to 503 K on a hot plate, held for 5−10 min to ensure melt isotropy, and then the pan was quickly quenched into liquid nitrogen to quench the sample to its glassy state. The glassy sample was transferred into the DSC, which was precooled to 253 K, then heated to the desired T_{iso}, between 323 and 373 K at the maximum instrumental heating rate of ~100° min^{-1}. When down-quenched to below about 418 K or up-quenched to above about 373 K, the sample began to crystallize before the isotherm was achieved and thus the crystallization heat flow could not be separated from the instrumental response. Heat-flow data were measured at T_{iso}, until crystallization was complete, typically between 1 and 100 min. The time scale of the raw heat-flow data was adjusted such that the time the quench initiated for each experiment occurred at t = 0 min. For both hot and cold crystallization, experiments were typically repeated three to five times for each sample at each isotherm.

The instrumental quench response (IQR) must be subtracted from the raw signal to obtain the crystallization heat flow. The IQR is primarily dependent upon the sample mass, but instrumental response as a function of T_{iso} is also observed. For hot crystallization, the IQR of an isotherm for which crystallization was well separated in time from the quench (e.g., $T_{iso} \geq 433$ K) was fit with a combination of two Gaussian and one Lorentzian functions. These Gaussian and Lorentzian parameters were then used as the starting parameters to fit the data using SOLVER46 to obtain the IQR for subsequent reactions of the same sample at different isotherms. For cold crystallization, the IQR was obtained by repeating the same cold → up-quench process for the crystallized sample immediately following the initial glass-to-crystal measurement without removing the sample from the instrument.

Isothermal Crystallization: Temperature- and Time-Resolved X-ray Diffraction (TtXRD). Synchrotron diffraction data were obtained using methods analogous to that previously reported for d_0-crystallization measurements.[41] Data reported here for all isotopically substituted CZX-1 samples, as well as all cold crystallization data were obtained on beamline 11-ID-B (60 keV, λ = 0.2114 Å, collimated beam 0.5 × 0.5 mm^2) at the Advanced Phonon Source, Argonne National Laboratory. Samples were sealed into 0.7 mm I.D. fused silica capillaries (Charles Supper Co., Natrick, MA), melt-crystal-cycled between 313 and 503 K, and affixed to a single-axis goniometer head with epoxy. Data were collected in a Debye−Scherrer geometry at a sampling rate of 1 Hz, with each diffractogram hereafter referred to as a frame, using a 2048 × 2048 PerkinElmer silicon detector.[49] During crystallization experiments, the samples were oscillated 1.2° per frame, in synchronization with the duration of exposure to the X-ray beam, to illuminate a larger region of the sample. After each crystallization experiment was complete, a final image was taken with the sample oscillating 18° while being exposed in the X-ray beam for 15 s to evaluate a larger portion of the Ewald sphere as a measure of the total crystalline diffraction intensity. The wavelength and detector alignment were calibrated with a CeO_2 standard.

Quenching samples to a crystallization isotherm within a fraction of a second was achieved using an in-house-constructed dual-air-stream, quenching furnace (Figure S1, Supporting Information). Two 3/4 in. in-line air heaters (Omega), independently controlled using Eurotherm 91p programmable temperature controllers, are mounted on a pneumatically controlled carriage. Upon throwing the pneumatic switch, the $T_{initial}$ air stream is instantaneously replaced with the T_{iso} air stream. Controlling thermocouples were placed in the mouth of each air stream and also just above the sample being measured. The temperature was calibrated using the external calibrant of the phase transitions of elemental sulfur and the internal calibrant of the melting temperature of d_0-CZX-1. A temperature accuracy of ±2.5 °C was obtained; the relatively large range is a result of sample environment conditions including temperature gradients, variations in airflow, and sample/thermocouple placement within the air stream. While instantaneous quenching is preferred to obtain ideal isothermal kinetics, crystal growth kinetics were also measured with temperature programmed quenching at rates of 30 and 60° min^{-1} to evaluate the correlation between quench rate and nucleation density, required to correlate DSC and TtXRD data.

Hot crystallization experiments were performed by heating capillary samples, with 1−2 mm ingots of CZX-1, to 503 K for at least 5 min prior to quenching to the desired T_{iso}. For cold crystallization experiments, samples were melted in the high-temperature airflow and held at 503 K for at least 5 min to ensure melt isotropy; then, the high-temperature airflow was removed, and the sample was immediately frozen with a compressed air stream from an aerosol dust removal canister. The glass samples were then exposed to an up-quench from room temperature to the desired T_{iso} using the pneumatic forced air quenching furnace described above. For all quenching conditions, diffraction data collection was initiated at least 15 frames prior to the quench to T_{iso} and continued until crystallization was complete.

Analysis of bulk crystallization transformations was achieved by using fit2D[50] to azimuthally average the serial 2-D X-ray frames for each TtXRD measurement. This yields one-dimensional diffraction patterns, which were subsequently analyzed by singular value decomposition to obtain the time dependence of peak intensities, and further normalized into the fraction of the sample transformed, α, as previously described.[41]

The 2-D TtXRD frames afford analysis of individual crystallite data by measuring the time-dependent intensity of individual diffraction spots as opposed to the azimuthal averaging of all data. To accomplish this, we have written in-house software, RamDog,[51,52] whereby the second derivative of each pixel is evaluated in two dimensions using the Savitzky−Golay method.[53] The pixels with the most negative second derivatives of intensity correspond to centers of the diffraction spots. For each TtXRD kinetic measurement, the pixel coordinates of diffraction spots were selected from the final 2-D images and their corresponding integrated intensities evaluated for all frames of the kinetic run, the change in diffracted intensity being directly proportional to the growth of each corresponding crystallite. Accurately correlating the integrated intensity of individual diffraction spots to the size of the corresponding crystallite is nontrivial and is the subject

DOI: 10.1021/acs.jpcc.9b01334
J. Phys. Chem. C 2019, 123, 7475−7485

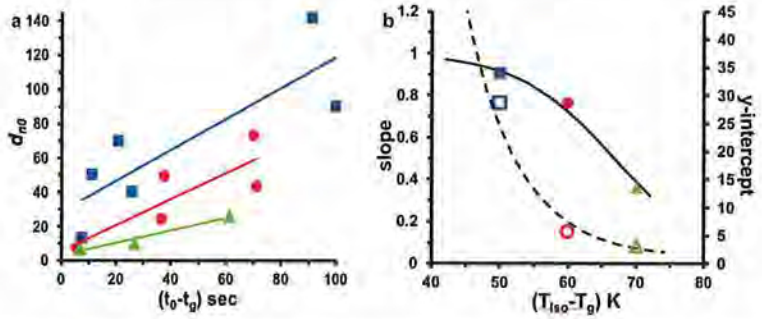

Figure 2. (a) Plot demonstrating the approximate linear correlation between d_{n_0} and $(t_0 - t_g)$ as a function of T_{iso} [353 K (blue squares), 363 K (red circles), and 373 (green triangles)] for TtXRD measurements of cold crystallization with various programmed up-quench rates. (b) The slopes (solid line and symbols) and y-intercepts (dashed line and open symbols) of the linear functions are empirically correlated to $T_{iso} - T_g$ by exponential functions, which yield the following empirical function for $d_{n_0(T_{iso})}$ for cold crystallization of CZX-1.

$$d_{n_0(T_{iso})} = \left[\frac{1}{1 + \exp(0.141(T_{iso} - T_g) - 9.4147)}\right](t_0 - t_g) + [1 + \exp(-0.1294(T_{iso} - T_g) + 9.6166)]$$

of ongoing work. However, to a first approximation, here we analyze the integrated intensity of the identified diffraction spots of the most intense (1, 1, 0), (2, 1, 1), (2, 2, 2), and (3, 2, 1) reflections. The intensity from the last frame (the completed transformation) is compared to the total diffraction intensity at the corresponding Q vector, which, when multiplicity-normalized and compared to the size of the total sample in the X-ray beam, provides an estimate of the number and size of crystallites.

RESULTS

Determining the Velocity of the Phase Boundary, v_{pb}. Both DSC and TtXRD data describe the time-dependent transformation of the melt to the crystalline material at a given isotherm. DSC methods afford better temperature control, finer time resolution, and, being in-house, are not time restricted for measurement of slow crystallization. But DSC methods are limited with respect to quench rates and are blind to separating growth from nucleation. Two-dimensional TtXRD methods with our quenching furnace afford excellent quenching rates, a unique ability to distinguish growth from nucleation, but have more limited time resolution and temperature sensitivity, and the availability of general user time on the synchrotron makes such measurement of slow reactions impractical.

The heat flow (DSC) or diffraction intensity (TtXRD) directly corresponds to the fraction of the sample transformed from the liquid to crystal, conventionally described as $\alpha(t)$. To extract physically meaningful mechanistic data from these measurements, however, it is necessary to normalize the $\alpha(t)$ data with respect to the amount of sample being measured. We previously demonstrated critical modifications to the classic, empirical Kolmogorov–Johnson–Mehl–Avrami (KJMA) condensed-matter rate expression that corrects for sample size and shape effects.[41,54] Our modified (M)-KJMA rate expression, eq 6, yields the physical velocity of the crystallization phase boundary, v_{pb}, as a rate constant (units of distance × time^{-1}) as opposed to the relative rate constant (units of time^{-1}) afforded by the KJMA expression.

$$\alpha(t) = 1 - \exp\left\{-\left[\frac{v_{pb}a_c}{g\sqrt[3]{V}}(t - t_0)\right]^{n'}\right\} \quad (6)$$

Here, t_0 is the time of nucleation, n' is the apparent crystal growth dimensionality, V is the sample volume, g describes the intrinsic crystal growth habit ($g = 1$ for isotropic growth), and a_c describes the anisotropy of the sample environment. The M-KJMA expression is a semiempirical expression, but its use as a means to extract the v_{pb} from bulk measurements has been validated by simulations[54] and by video measurement of the actual phase boundary velocity.[21]

In the present work, however, analysis of the bulk transformations indicated a dramatically faster apparent crystallization rate for cold than for hot crystallization. The 2-D TtXRD experiments also reveal that cold crystallization exhibits enhanced nucleation (see Figure S2, Supporting Information). To resolve the contrast between hot and cold crystallization, RamDog software[51,52] was developed to measure the time-dependent growth of individual crystallites, independent of nucleation, based on the growth of each diffraction spot normalized to the size of the corresponding individual crystallites, instead of to the bulk sample. The individual crystallite analysis demonstrates equivalent v_{pb}'s for both hot and cold crystallization (Figure S3, Supporting Information). These data confirm that enhanced nucleation, dividing the measured sample volume into smaller crystallite volumes, causes an enhanced apparent growth rate.

Because enhanced nucleation subdivides a sample into numerous smaller growth volumes, for bulk sample analysis (required for evaluation of the DSC data), the sample size must be corrected by V/n_0, where n_0 is the number of initial nuclei. Fortunately, the individual crystallite analysis by 2-D TtXRD methods affords measurement of the nucleation density ($d_{n_0} = n_0/V$), which, to a first approximation, is a scale factor to determine the number of initial nuclei in the larger DSC samples.

Multiple factors including T_{iso} and the quenching rate impact the number of crystallites that nucleate in a sample. Repeated TtXRD experiments exhibit significant variation in

DOI: 10.1021/acs.jpcc.9b01334
J. Phys. Chem. C 2019, 123, 7475−7485

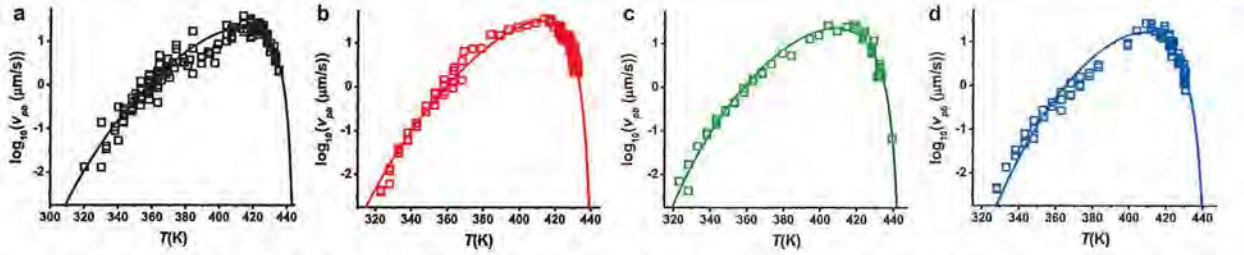

Figure 3. Experimental $v_{pb}(T)$ data for (a) d_0- (black), (b) d_1- (red), (c) d_9- (green), and (d) d_{10}-CZX-1 (blue). Solid lines represent the best fit to eq 4.

the number of crystallites formed from reactions quenched to equivalent T_{iso}. However, the parameter that appears to be the most consistently correlated with the number of crystallites is the time between when the sample is heated past its glass-transition temperature, t_g, and the time when crystal growth is first observed, t_0. As shown in Figure 2a, the initial nucleation density, d_{n_0}, for cold crystallization at the same T_{iso} increases in an approximately linear fashion with respect to $(t_0 - t_g)$. Albeit with a limited set of data, the respective slopes and y-intercepts of these lines suggest an empirical, exponential relationship with respect to $T_{iso} - T_g$; Figure 2b. This empirical relationship, given in the caption of Figure 2, should not be overinterpreted or applied to conditions far outside the measured temperature ranges. The slope should never become negative, but it is anticipated to approach zero as T_{iso} approaches T_{max}. The y-intercepts, which must be ≥ 1, may indicate the number of germ nuclei at the given T_{iso}.Using the known size of DSC samples, along with this empirical relationship between d_{n_0} and $(t_0 - t_g)$ observed from the data in Figure 2, it is possible to obtain a reasonable estimate of the number of initial nuclei, n_0, in the isothermal DSC cold crystallization measurements. Replacing V in eq 6 with V/n_0 yields the systems intrinsic v_{pb}, which is observed to be indistinguishable for hot and cold crystallization using either the DSC or TtXRD method (Figure S3, Supporting Information).

Crystal Growth Rates of d_0-, d_1-, d_9- and d_{10}-CZX-1. Using the DSC and TtXRD methods described above to determine the v_{pb} by hot and cold crystallization, the temperature-dependent crystal growth rates were measured for CZX-1 with each of the d_0, d_1, d_9, and d_{10} isotopically substituted trimethylammonium templates. The temperature-dependent v_{pb} data for each isotopic substitution is shown in Figure 3 (the $v_{pb}(T)$ data is provided in Tables T1–T4, Supporting Information). The resulting experimental $v_{pb}(T)$ data was then fit to the TZT_c function, eq 4, using nonlinear least-squares methods to obtain the activation parameters reported in Table 1.

DISCUSSION

The d_0-, d_1-, d_9-, and d_{10}-$[(H/D)N(C(H/D)_3)_3]^+$ isotopic substitutions exhibit subtle but statistically significant variation in their respective rates of crystal growth of CZX-1. The comparative $v_{pb}(T)$ functions are plotted in Figure 4. Notably, the difference in observed rates due to isotopic effects at any single T_{iso} is indistinguishable from experimental error. This is particularly true given that, as demonstrated by M-KJMA analysis of simulations,[54] without knowledge of the precise location of nucleation within the sample, the v_{pb} only can be identified to within a factor of 2 of the accurate value. However, the temperature dependence of the $v_{pb}(T)$ for each system, measured over almost the full temperature range between T_m and T_g, delineates statistically unique activation parameters for each isotopic system.

Notably, because of the non-Arrhenius temperature dependence of this condensed-matter reaction, it is not possible to obtain useful information from a typical k_H/k_D ratio of rate constants. Instead, isotope effects on both the thermodynamic parameters T_m and T_K as well as the kinetic activation parameters ΔH_c^*, ΔS_c^*, and z_c must be evaluated. Here, isotopic effects are considered with respect to the relative moment of inertia (rMoI) of the templating cation, instead of its mass, since H/D substitution at the N–H position is closer to the molecular ion's center of mass than H/D substitution of the methyl hydrogens, and the templating cation is off-center from the center of the metal–halide cage. As seen in Table 1, there is no statistically significant difference between the melting points of isotopomers. By contrast, T_K, ΔH_c^*, ΔS_c^*, and z_c vary significantly between isotopomers, as shown in the

Table 1. Material and Activation Parameters for Crystal Growth of CZX-1. Standard Errors in Parentheses

CZX-1	d_0	d_1	d_9	d_{10}
a (Å)[a]	10.5887(3)	10.559(9)	10.570(2)	10.563(12)
T_m (K)	446(2)	448(2)	447(1)	446(2)
T_K (K)	150	157	203	213
rMoI	1.0	1.04	1.22	1.26
ΔH_c^* (kJ mol^{-1})	37.7(4)	38.74(12)	26.8(2)	27.1(2)
ΔS_c^* (J mol^{-1} K^{-1})	−8(1)	−1.6(2)	−16(1)	−11(1)
z_c	0.58(4)	1.13(4)	0.53(2)	0.68(3)

[a]By single-crystal XRD at 100 K for d_0-CZX-1 and RT PXRD for d_1-, d_9-, and d_{10}-CZX-1.

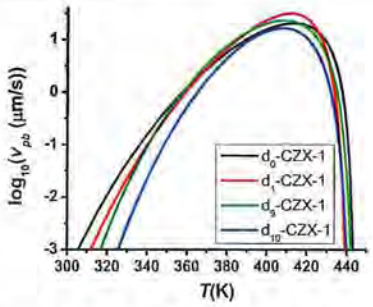

Figure 4. Composite of the CZX-1 $v_{pb}(T)$ crystal growth functions for each of the d_0, d_1, d_9, and d_{10} isotopic substitutions of the trimethylammonium templating cations.

DOI: 10.1021/acs.jpcc.9b01334
J. Phys. Chem. C 2019, 123, 7475–7485

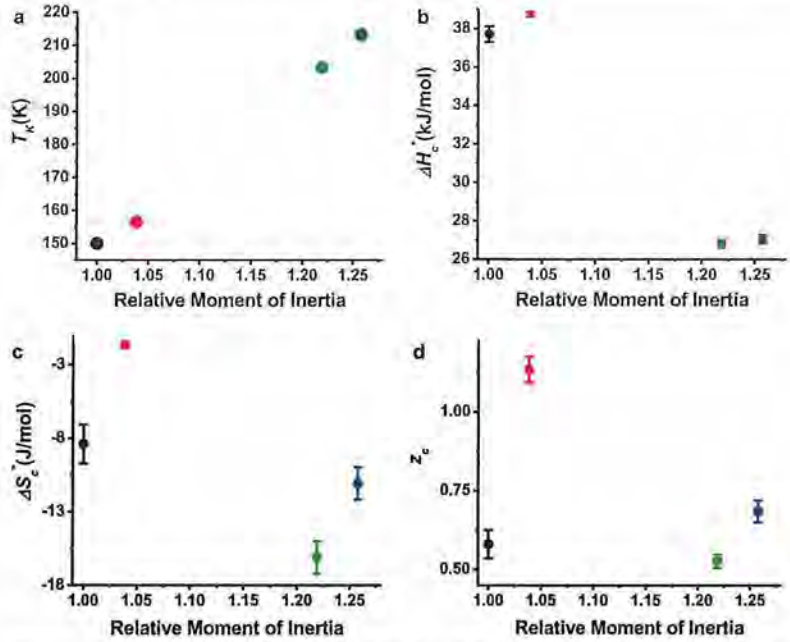

Figure 5. Isotope effects for the crystallization of d_0-, d_1-, d_9-, and d_{10}-CZX-1 including (a) the thermodynamic T_K and kinetic (b) ΔH_c^*, (c) ΔS_c^*, and (d) z_c parameters, plotted with respect to the rMoI of the templating cation. Error bars represent ± 1 standard deviation.

plots of Figure 5, with each parameter being larger (more positive) for the N–D substitution and smaller (more negative) for CD_3 substitution.

Template Inertial (Mass) Effects. As a first approximation, the template–cage interaction may be modeled by the rotational and vibrational modes between the template and the cage. The energy levels and the difference between energy levels of rotational and vibrational modes should be inversely proportional to the reduced mass. Therefore, similar to the H/D isotope effect in molecular systems,[55,56] the increased template mass, and thus the increased reduced mass, leads to lower and more narrowly spaced rotational and vibrational energy levels.

The linear correlation of T_K to the rMoI of the template suggests that this may be due to the lower energy and higher density of the configurational microstates associated with the heavier isotopomers. As such, the supercooled liquid begins to take on characteristics of bands, like would be found in the crystalline state, at a higher temperature for heavier isotopomers. Thus, complete cooperativity, i.e., T_K, occurs at a significantly higher temperature for d_{10}-CZX-1 than for the d_0 isotopomer.

The lowering and condensation of vibrational and rotational energy levels also suggest that at any given temperature, higher energy levels can be populated for liquids of heavier isotopomers, thus lowering the enthalpic barrier for template reorganization. This is consistent with the smaller ΔH_c^* parameters for the d_9- and d_{10}-isotopomers as compared to the lighter d_0- and d_1-materials.

Similarly, the higher entropy associated with more accessible microstates for heavier isotopomers in their reactant supercooled liquid should decrease the ratio of transition and reactant configurations, $W^{\ddagger}/W_{rctv}$ resulting in a more negative ΔS_c^*. As shown in Figure 5c, controlling for the NH– versus ND–framework hydrogen bonding, the ΔS_c^* of d_9-CZX-1 is significantly more negative than that of d_0-CZX-1. A similar relationship is observed comparing d_{10}- and d_1-CZX-1. The z_c parameter, which, as described above, is correlated to ΔS_c^*,[20] exhibits analogous isotope effects.

Hydrogen-Bonding Effects. Notably, the isotope effects for ΔH_c^*, ΔS_c^*, and z_c parameters do not exhibit the linear correlation with respect to the template rMoI as was observed for T_K. For these parameters, the d_0 and d_9 isotopomers each exhibit smaller (more negative) values than are observed for the d_1 and d_{10} isotopomers, respectively, suggesting differential NH– versus ND–framework hydrogen-bond effects.

The positive value of ΔH_c^* for all isotopomers suggests that bonding is diminished to access the transition zone for crystallization. The slight increase in ΔH_c^* when the N–H is replaced with N–D suggests that in this system deuterium bonding is slightly stronger than hydrogen bonding. The 0.3–1.0 kJ mol^{-1} difference in ΔH_c^* between NH and ND isotopomers is consistent with literature reports of the measured/calculated difference in hydrogen versus deuterium bonding.[57,58]

ΔS_c^* is negative for all isotopomers, consistent with the required organization into long-range order of a crystallization reaction. However, d_1- and d_{10}-CZX-1 exhibit significantly less negative values of ΔS_c^* than are observed for the d_0 and d_9 materials. The less negative ΔS_c^* for the N–D substitutions is consistent with the stronger N–D–framework interaction forming a more ordered reactant liquid that requires less rearrangement to achieve the crystallization transition zone. Again the correlation between ΔS_c^* and z_c[20] results in similar trends to the z_c parameter. Importantly, larger z_c leads to greater temperature dependence of the activation entropy.

Combined Thermodynamic and Kinetic Rate Effects. Perhaps the most unique distinguishing feature between condensed-matter reactions, such as crystal growth, and reactions in dilute media is the impact of cooperativity on the reaction system. In dilute media, the transition state is a result of the collision between the same number of discreet

DOI: 10.1021/acs.jpcc.9b01334
J. Phys. Chem. C 2019, 123, 7475–7485

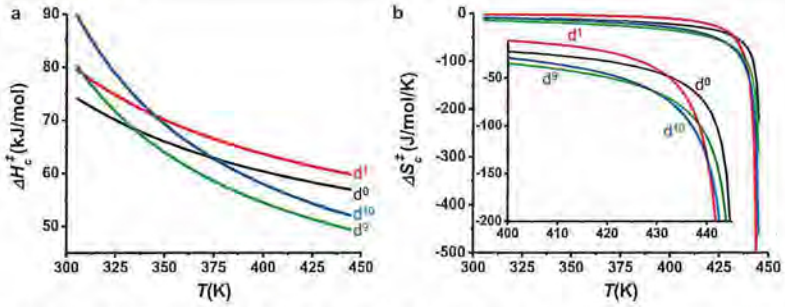

Figure 6. Temperature-dependent (a) $\Delta H_c^{\ddagger}$ and (b) $\Delta S_c^{\ddagger}$ for d_0- (black), d_1- (red), d_9- (green), and d_{10}-CZX-1 (blue). Inset in (b) expands the plotted temperature region between 400 and 445 K.

particles irrespective of the reaction temperature. By contrast, in the condensed phase, there are no independent reacting species. Instead, the relative size of the ensemble of interacting units that form the transition zone is dependent on the temperature of the system, i.e., there is greater cooperativity at lower temperature.[34] It is the change in the cooperativity within the reacting system that causes condensed-matter reactions to exhibit non-Arrhenius kinetic behavior. Because the cooperativity of units forming the transition zone is temperature dependent, the temperature dependence of $\Delta H_c^{\ddagger}(T)$ and $\Delta S_c^{\ddagger}(T)$ must be evaluated; Figure 6.[20]

At higher reaction temperatures, $T \gg T_K$, the cooperativity diminishes such that the $\Delta H_c^{\ddagger} \rightarrow \Delta H_c^*$. Here, hydrogen-bonding effects are significant, resulting in the order of $\Delta H_c^{\ddagger}$ $d_1 > d_0$ and $d_{10} > d_9$. However, as T approaches T_K, the effect of the rMoI on the Kauzmann temperature dominates the relative order of the $\Delta H_c^{\ddagger}$, with $d_0 < d_1 < d_9 < d_{10}$.

For $\Delta S_c^{\ddagger}$, stronger ND−framework interactions at low temperature reduce W_{rct} and thus increase $W^{\ddagger}/W_{rct}$, causing the d_1- and d_{10}-isotopomers to exhibit less negative values for $\Delta S_c^{\ddagger}$ than for d_0- and d_9-CZX-1. At high temperature, W_{rct} is large for both H and D substitutions. However, stronger ND−framework interactions also result in fewer transition configurations, $W^{\ddagger}$, thus decreasing $W^{\ddagger}/W_{rct}$ and magnifying the effect of the temperature-dependent change in W_{rct}. As a result, at elevated temperatures, the $\Delta S_c^{\ddagger}$ for the d_1 and d_{10} materials becomes the most negative.

CONCLUSIONS

Investigating the temperature-dependent crystallization rates of the sodalite-type material CZX-1 utilizing a systematic isotopic substitution of the $[(H/D)N(C(H/D)_3)_3]^+$ templating cation provides unique insight into the intrinsic role of template−framework interactions on the rate of crystal growth. As is well established by measuring KIE of molecular reactions, variation in the reaction rates as a function of isotopic substitution gives clear indication as to whether or not the isotopically substituted species are directly involved in the formation of the activated complex(es), which control the rate-limiting step of the reaction. The above-described temperature dependence of the $\Delta H_c^{\ddagger}(T)$ and $\Delta S_c^{\ddagger}(T)$ yields a temperature-dependent free energy of activation, $(\Delta G_c^{\ddagger}(T) = \Delta H_c^{\ddagger}(T) - T\Delta S_c^{\ddagger}(T))$, that results in a variable k_H/k_D ratio, depending on the reaction temperature (see Figure 4). By contrast, TZT_c analysis of the T_K and ΔH_c^*, ΔS_c^*, and z_c activation parameters for crystallization rates d_0- to d_{10}-CZX-1 isotopomers reveal intrinsic isotope effects that provide direct insight into the reaction mechanism.

Specifically comparing the impact on the crystallization rate of the rMoI (mass) of the template $\{d_0$ and d_1 vs d_9 and $d_{10}\}$ and the NH versus ND hydrogen-bonding ability $\{d_0$ and d_9 vs d_1 and $d_{10}\}$ reveals the extent to which template reorientation and hydrogen bonding between the template and framework, respectively, influence the rate of crystal growth. The melting temperature, T_m, is not significantly impacted by any of the isotopic substitutions. By contrast, the Kauzmann temperature, T_K, demonstrates a linear dependence with respect to the rMoI, indicating that it is not significantly impacted by hydrogen bonding. The activation enthalpic and entropic activation parameters, ΔH_c^* and ΔS_c^*, respectively, demonstrate both inertial and hydrogen-bonding isotope effects, both indicating that ND−framework deuterium bonding is stronger than NH−framework hydrogen bonding.

This alkylammonium templated metal−halide framework is a unique system; thus, there are limits to the extent to which mechanistic conclusions can be applied to other templated network systems. However, it is reasonable to predict that while the magnitude of the influences will be system dependent, the overall mechanistic picture, which demonstrates that template reorientation, including impacts from both the template−cage interaction and the inertia of the entire template, plays significant roles in the activation process of crystal growth, should be generally applicable to diverse systems. In addition, this novel isotope effect study based on the transition zone theory introduces an important tool that can be used to evaluate the mechanism(s) of other condensed-matter reactions.

ASSOCIATED CONTENT

Supporting Information

The Supporting Information is available free of charge on the ACS Publications website at DOI: 10.1021/acs.jpcc.9b01334.

Description of the dual-air stream quenching furnace (Figure S1); exemplar 2-D diffraction images demonstrating differential nucleation for hot and cold crystallization (Figure S2); plot of ν_{pb} vs T for crystal growth of d_0-CZX-1 demonstrating equivalence of data from both DSC and TtXRD methods and from both hot and cold crystallization (Figure S3); $\nu_{pb}(T)$ for each isotopomer (Tables T1−T4) (PDF)

AUTHOR INFORMATION

Corresponding Author

*E-mail: Jim_Martin@NCSU.edu.

DOI: 10.1021/acs.jpcc.9b01334
J. Phys. Chem. C 2019, 123, 7475−7485

ORCID

Feier Hou: 0000-0002-6314-0129

James D. Martin: 0000-0001-7414-2683

Notes

The authors declare no competing financial interest.

■ ACKNOWLEDGMENTS

This work was supported by NSF via contracts DMR-0705190 and DMR-1709370. This research used resources of the Advanced Photon Source, a U.S. Department of Energy (DOE) Office of Science User Facility operated for the DOE Office of Science by Argonne National Laboratory under Contract No. DE-AC02-06CH11357.

■ ABBREVIATIONS

TZT_c, transition zone theory of crystallization; CZX-1, $[HNMe_3]CuZn_5Cl_{12}$; T_K, Kauzmann temperature; KIE, kinetic isotope effect; k_H, k_D, rate constants with H vs D substitution; T_{max}, temperature of the maximum crystal growth rate; T_g, glass-transition temperature; T_m, normal melting point; TtXRD, time temperature X-ray diffraction; DSC, differential scanning calorimetry; ICG, interface controlled growth model of crystallization; r_a, r_d, rate of attachment or detachment; ν, frequency; T, temperature; R, gas constant; $\Delta G_a^{\ddagger}$, free energy of activation for attachment; ΔG_c, free energy difference between liquid and crystal; Y, growth rate as defined by ICG; a_0, thickness of a molecular layer; f, fraction of sites on a crystal surface; $\Delta H^{\ddagger}$, enthalpy of activation; $\Delta S^{\ddagger}$, entropy of activation; k_B, Boltzmann's constant; η, viscosity; TST, transition state theory; h, Plank's constant; TZ, transition zone; λ, characteristic wavelength of vibrations that leads to crystal growth, equal to 2 times the average lattice constant; S_{liq}, S_{xtl}, configurational entropy of the liquid and crystal, respectively; $W^{\ddagger}$, W_{rct}, number of configurations of the TZ and reactant, respectively; ΔS_c^*, intrinsic (i.e., temperature-independent) component of the entropy of activation; z_c, fitting parameter of TZT_c that modulates the temperature dependence of $\Delta S^{\ddagger}$, approximately equal to $-R/\Delta S^*$; ΔH_c^*, intrinsic (i.e., temperature-independent) component of the enthalpy of activation; v_{pb}, velocity of the crystallization phase boundary; PXRD, powder X-ray diffraction; TMDSC, temperature-modulated differential scanning calorimetry; C_p, heat capacity; ΔC_p, difference in heat capacity of liquid and crystalline phases; ΔH_m, enthalpy of melting; T_{iso}, isothermal temperature of crystallization reaction; IQR, instrumental quench response; α, fraction of the sample transformed from the liquid to crystalline phase; KJMA, Kolmogorov–Johnson–Mehl–Avrami rate expression; M-KJMA, modified KJMA expression; t_0, time of nucleation; n, dimensionality of crystal growth; V, sample volume; g, intrinsic crystal growth habit (g = 1 for isotropic growth); a_c, anisotropy correction for the sample environment; n_0, number of initial nuclei; d_{n_0}, initial nucleation density; t_g, when ramping up in temperature, time between initiation of the quench and when the sample reaches T_g; rMoI, relative moment of inertia

■ REFERENCES

(1) Bohm, J. The History of Crystal Growth. *Acta Phys. Hung.* **1985**, *57*, 161–178.

(2) Dandekar, P.; Kuvadia, Z. B.; Doherty, M. F. Engineering Crystal Morphology. *Annu. Rev. Mater. Res.* **2013**, *43*, 359–386.

(3) Shtukenberg, A. G.; Punin, Y. O.; Gunn, E.; Kahr, B. Spherulites. *Chem. Rev.* **2012**, *112*, 1805–1838.

(4) Meldrum, F. C.; Cölfen, H. Controlling Mineral Morphologies and Structures in Biological and Synthetic Systems. *Chem. Rev.* **2008**, *108*, 4332–4432.

(5) Sear, R. P. The non-classical nucleation of crystals: microscopic mechanisms and applications to molecular crystals, ice and calcium carbonate. *Int. Mater. Rev.* **2012**, *57*, 328–356.

(6) De Yoreo, J. J.; Gilbert, P. U. P. A.; Sommerdijk, N. A. J. M.; Penn, R. L.; Whitelam, S.; Joester, D.; Zhang, H.; Rimer, J. D.; Navrotsky, A.; Banfield, J. F.; Wallace, A. F.; Michel, F. M.; Meldrum, F. C.; Cölfen, H.; Dove, P. M. Crystallization by particle attachment in synthetic, biogenic, and geologic environments. *Science* **2015**, No. aaa6760.

(7) Aizenberg, J. Crystallization in Patterns: A Bio-Inspired Approach. *Adv. Mater.* **2004**, *16*, 1295–1302.

(8) Rimer, J. D.; An, Z.; Zhu, Z.; Lee, M. H.; Goldfarb, D. S.; Wesson, J. A.; Ward, M. D. Crystal Growth Inhibitors for the prevention of L-Cystine Kidney Stones Through Molecular Design. *Science* **2010**, *330*, 337–341.

(9) Davey, R. J. The Role of the solvent in crystal growth from solution. *J. Cryst. Growth* **1986**, *76*, 637–644.

(10) Treivus, E. B. Solvent effect on the kinetics of crystal growth. *Russ. Chem. Rev.* **1992**, *61*, 673–682.

(11) Lahav, M.; Leiserowitz, L. A stereochemical approach that demonstrates the effect of solvent on the growth of polar crystals: a perspective. *Cryst. Growth Des.* **2006**, *6*, 619–624.

(12) Anderson, M. D.; Thompson, J. O.; Johnson, D. C. Avoiding Binary Compounds as Reaction Intermediates in Solid State Reactions. *Chem. Mater.* **2013**, *25*, 3996–4002.

(13) Kuech, T. F., Ed.; *Handbook of Crystal growth: Thin Films and Epitaxy: Basic Techniques*; Elsevier: New York, 2015; Vol. *III*, Part A.

(14) Tranchemontagne, D. J.; Mendoza-Cortéz, J. L.; O'Keeffe, M.; Yaghi, O. M. Secondary building units, nets and bonding in the chemistry of metal-organic frameworks. *Chem. Soc. Rev.* **2009**, *38*, 1257–1283.

(15) Baerlocher, C.; McCusker, L. B.; Olson, D. H. *Atlas of Zeolite Framework Types*, 6th ed.; Elsevier: New York, 2007.

(16) O'Hare, D.; Walton, R. I. An in Situ Energy-Dispersive X-ray Diffraction Study of the Hydrothermal Crystallization of Zeolite A. 2. Effect of Deuteration on Crystallization Kinetics. *J. Phys. Chem. B* **2001**, *105*, 91–96.

(17) Dunitz, J. D. The Entropic Cost of Bound Water in Crystals and Biomolecules. *Science* **1994**, *264*, 670.

(18) Vekilov, P. G. What is the Molecular-Level Role of the Solution Components in Protein Crystallization? *Cryst. Growth Des.* **2007**, *7*, 2239–2246.

(19) Tidhar, Y.; Weissman, H.; Tworowski, D.; Rybtchinski, B. Mechanism of Crystalline Self-Assembly in Aqueous Medium: A Combined Cryo-TEM/Kinetic Study. *Chem. – Eur. J.* **2014**, *20*, 10332–10342.

(20) Hou, F.; Martin, J. D.; Dill, E. D.; Folmer, J. C. W.; Josey, A. A. Transition Zone Theory of Crystal Growth and Viscosity. *Chem. Mater.* **2015**, *27*, 3526–3532.

(21) Hillis, B. G.; Losey, B. P.; Weng, J.; Ghaleb, N.; Hou, F.; Martin, J. D. From Rate Measurements to Mechanistic Data for Condensed Matter Reactions: A case study using the crystallization of $[Zn(OH_2)_6][ZnCl_4]$. *Crystals* **2017**, *7*, 1–16.

(22) Collins, C. J.; Bowman, N. S. *Isotope Effects in Chemical Reactions*; Van Nostrand Reinhold: New York, 1971.

(23) Dutta, P. K.; Puri, M.; Bowers, C. *Influence of D_2O and Alcohols on the Crystallization of Zeolites*; ACS Symposium Series; ACS, 1989; Vol. *398*, pp 98–109.

(24) Kirichek, O.; Soper, A.; Dzyuba, B.; Callear, S.; Fuller, B. Strong Isotope Effects on Melting Dynamics and Ice Crystallization Processes in Cryo Vitrification Solutions. *PLoS One* **2015**, *10*, No. e0120611.

(25) Johari, G. P.; Hallbrucker, A.; Mayer, E. Isotope effect on the glass transition and crystallization of hyperquenched water. *J. Chem. Phys.* **1990**, *92*, 6742–6746.

DOI: 10.1021/acs.jpcc.9b01334
J. Phys. Chem. C 2019, 123, 7475–7485

(26) Eyring, H. J. The Activated Complex in Chemical Reactions. *J. Chem. Phys.* **1935**, *3*, 107–115.
(27) Wilson, H. W. XX. On the Velocity of Solidification and Viscosity of supercooled liquids. *London, Edinburgh Dublin Philos. Mag. J. Sci.* **1900**, *50*, 238–250.
(28) Kirkpatrick, R. J. Crystal growth from the melt: a review. *Am. Mineral.* **1975**, *60*, 798–814.
(29) Martin, J. D.; Greenwood, K. B. Halo-Zeotypes: A New Generation of Zeolite-type Materials. *Angew. Chem., Int. Ed.* **1997**, *36*, 2072–2075.
(30) Martin, J. D.; Goettler, S. J.; Fosse, N.; Iton, L. Designing Intermediate Range Order in Amorphous Materials. *Nature* **2002**, *419*, 381–384.
(31) Josey, A. A. The Structure and Mechanism of Melt Crystallization of CZX-1, A Templated $ZnCl_2$ Network Material. Thesis under the Direction of J. D. Martin, NCSU, 2008.
(32) Salmon, P. S.; Martin, R. A.; Mason, P. E.; Cuello, G. J. Topological versus chemical ordering in network glasses at intermediate and extended length scales. *Nature* **2005**, *435*, 75–78.
(33) Kauzmann, W. The Nature of the Glassy State and the Behavior of Liquids at Low Temperatures. *Chem. Rev.* **1948**, *43*, 219–256.
(34) Adam, G.; Gibbs, J. H. On the Temperature Dependence of Cooperative Relaxation Properties in Glass-Forming Liquids. *J. Chem. Phys.* **1965**, *43*, 139–146.
(35) Fine, M. E. *Introduction to Phase Transformations in Condensed Systems*; Macmillan Co.: New York, 1964.
(36) Turnbull, D.; Cohen, M. H. Crystallization Kinetics and Glass Formation. In *Modern Aspects of the Viterous State*; MacKenzie, S. D., Ed.; Butterworths: London, 1960; Vol. 38–62.
(37) Simmons, J. H.; Uhlmann, D. R. et al. *Nucleation and Crystallization of Glasses*; Advances in Ceramics; American Ceramic Society: Ohio, 1982; Vol. *4*.
(38) Jackson, K. A.; Uhlmann, D. R.; Hunt, J. D. On the nature of crystal growth from the melt. *J. Cryst. Growth* **1967**, *1*, 1–36.
(39) An, H.; Li, X.; Geng, Y.; Wang, Y.; Wang, X.; Li, L.; Li, Z.; Yang, C. Shear-induced conformational ordering, relaxation, and crystallization of isotactic polypropylene. *J. Phys. Chem. B* **2008**, *112*, 12256–12262.
(40) Martin, J. D.; Hou, F. Transition Zone Theory of the Glass Transition. *J. Non-Cryst. Solids* **2018**, *491*, 24–33.
(41) Dill, E. D.; Josey, A. A.; Folmer, J. C. W.; Hou, F.; Martin, J. D. Experimental Determination of the Crystallization Phase-Boundary Velocity in the Halozeotype CZX-1. *Chem. Mater.* **2013**, *25*, 3932–3940.
(42) Galwey, A. K.; Brown, M. E. A theoretical justification for the application of the Arrhenius equation to kinetics of solid state reactions (mainly ionic crystals). *Proc. R. Soc. London, Ser. A* **1995**, *450*, 501–512.
(43) Šesták, J. J. Rationale and fallacy of thermoanalytical kinetic patterns. *Therm. Anal. Calorim.* **2012**, *110*, 5–16.
(44) Hillis, B. G.; Martin, J. D. Transition Zone Theory of Crystallization: A Unifying Theory for Phase Boundary Controlled Crystal Growth Applied to a Series of Inorganic Glass-Forming Materials, in preparation, 2019.
(45) Nascimento, M. L. F.; Zanotto, E. D. Does viscosity describe the kinetic barrier for crystal growth from the liquidus to the glass transition? *J. Chem. Phys.* **2010**, *133*, No. 174701.
(46) Kauffman, G. B.; Fang, L. Y.; Viswanathan, N.; Townsend, G. Purification of Copper(I) Iodide. In *Transition Metal Complexes and Compounds*; Holt, S. L., Jr., Ed.; Inorganic Syntheses; Inorganic Syntheses, Inc., 1983; Vol. 22, pp 101–103.
(47) Zhou, D.; Zhang, G. G. Z.; Law, D.; Grant, D. J. W.; Schmitt, E. A. Physical stability of amorphous pharmaceuticals: Importance of configurational thermodynamic quantities and molecular mobility. *J. Pharm. Sci.* **2002**, *91*, 1863–1872.
(48) Thompson, C. V.; Spaepen, F. Approximation of the Free-Energy Change on Crystallization. *Acta Metall.* **1979**, *27*, 1855–1859.
(49) Chupas, P. J.; Chapman, K. W.; Lee, P. L. Applications of an amorphous silicon-based area detector for high-resolution, high-sensitivity and fast time-resolved pair distribution function measurements. *J. Appl. Crystallogr.* **2007**, *40*, 463–470.
(50) Hammersley, A. P.; Svensson, S. O.; Hanfland, M.; Fitch, A. N.; Hausermann, D. Two-Dimensional Detector Software: From Real Detector to Idealized Image or Two-Theta Scan. *High Pressure Res.* **1996**, *14*, 235–248.
(51) Dill, E. D. Determining Melt-Crystallization Mechanisms and Structures of Disordered Crystalline Solids. Thesis under the Direction of J. D. Martin, NCSU, 2013.
(52) Dill, E. D.; Folmer, J. C. W.; Martin, J. D. *RamDog: A Graphical User Interface Program to Interactively Analyze 2D Diffraction Images*, version 1.01; ZENDO, 2014.
(53) Savitzky, A.; Golay, M. J. E. Smoothing and differentiation of data by simplified least squares procedures. *Anal. Chem.* **1964**, *36*, 1627–1639.
(54) Dill, E. D.; Folmer, J. C. W.; Martin, J. D. Simulating crystallization to elucidate the parameter space in the KJMA condensed phase transformation model. *Chem. Mater.* **2013**, *25*, 3941–3951.
(55) Nordman, C. E.; Lipscomb, W. N. Note on the Hydrogen-Deuterium Isotope Effect in Crystals. *J. Chem. Phys.* **1951**, *19*, 1422.
(56) Rundle, R. E. The Deuterium Effect on Hydrogen Bond Distances in Crystals. *J. Chem. Phys.* **1953**, *21*, 937–938.
(57) Buckingham, A. D.; Fan-Chen, L. Differences in the Hydrogen and Deuterium Bonds. *Int. Rev. Phys. Chem.* **1981**, *1*, 253–269.
(58) Scheiner, S.; Cuma, M. Relative Stability of Hydrogen and Deuterium Bonds. *J. Am. Chem. Soc.* **1996**, *118*, 1511–1521.

DOI: 10.1021/acs.jpcc.9b01334
J. Phys. Chem. C 2019, 123, 7475–7485